

University of Groningen

Modulating the Verwey Transition of Epitaxial Magnetite Thin Films by Ionic Gating

Hou, Yanliang; Liu, Yang; Yang, Xuxin; Mao, Hongying; Shi, Zhong; Wu, Shuxiang; Lu, Bin; Ye, Quan Lin; Ye, Jianting

Published in:
Advanced Functional Materials

DOI:
[10.1002/adfm.202104816](https://doi.org/10.1002/adfm.202104816)

IMPORTANT NOTE: You are advised to consult the publisher's version (publisher's PDF) if you wish to cite from it. Please check the document version below.

Document Version
Publisher's PDF, also known as Version of record

Publication date:
2021

[Link to publication in University of Groningen/UMCG research database](#)

Citation for published version (APA):

Hou, Y., Liu, Y., Yang, X., Mao, H., Shi, Z., Wu, S., Lu, B., Ye, Q. L., & Ye, J. (2021). Modulating the Verwey Transition of Epitaxial Magnetite Thin Films by Ionic Gating. *Advanced Functional Materials*, 31(47), [2104816]. <https://doi.org/10.1002/adfm.202104816>

Copyright

Other than for strictly personal use, it is not permitted to download or to forward/distribute the text or part of it without the consent of the author(s) and/or copyright holder(s), unless the work is under an open content license (like Creative Commons).

The publication may also be distributed here under the terms of Article 25fa of the Dutch Copyright Act, indicated by the "Taverne" license. More information can be found on the University of Groningen website: <https://www.rug.nl/library/open-access/self-archiving-pure/taverne-amendment>.

Take-down policy

If you believe that this document breaches copyright please contact us providing details, and we will remove access to the work immediately and investigate your claim.

Downloaded from the University of Groningen/UMCG research database (Pure): <http://www.rug.nl/research/portal>. For technical reasons the number of authors shown on this cover page is limited to 10 maximum.

Modulating the Verwey Transition of Epitaxial Magnetite Thin Films by Ionic Gating

Yanliang Hou, Yang Liu, Xuxin Yang, Hongying Mao, Zhong Shi, Shuxiang Wu, Bin Lu, Quan-Lin Ye,* and Jianting Ye*

Understanding the Verwey transition in magnetite (Fe_3O_4), a strongly correlated magnetic oxide, is a one-century-old topic that recaptures great attention because of the recent spectroscopy studies revealing its orbital details. Here, the modulation of the Verwey transition by tuning the orbital configurations with ionic gating is reported. In epitaxial magnetite thin films, the insulating Verwey state can be tuned continuously to be metallic showing that the low-temperature trimeron states can be controllably metalized by both the gate-induced oxygen vacancies and proton doping. The ionic gating can also reverse the sign of the anomalous Hall coefficient, indicating that the metallization is associated with the presence of a new type of carrier with competing spin. The variable spin orientation associated with the sign reversal is originated from the structural distortions driven by the gate-induced oxygen vacancies.

transport, is caused by a first-order phase transition associated with a complex structural distortion from cubic (space group $Fd\bar{3}m$) to a monoclinic superstructure (space group Cc).^[3] The physical mechanism of this transition has been a decades-old puzzle ever since the Verwey's first proposal of charge ordering of Fe^{2+} and Fe^{3+} ions on the B sites.^[3] Recently, the low-temperature insulating phase has been identified as a trimeron network formed by a linear three-Fe-site unit with the minority-spin t_{2g} electrons of the Fe^{2+} ion delocalized at the center. The charge-density spreading of the Fe^{2+} ions to the two neighboring B -site Fe^{3+} ions at the apex is accompanied by shortening the


Fe–Fe distance.^[4] When the temperature increases, the trimers become mobile before melting at Verwey transition temperature T_v . Correspondingly, the magnetite transforms from a Verwey insulating state to a metallic phase.^[5,6]

Suggested by its orbital origin, external modulations that can change the orbital details such as, chemical doping,^[7] strain,^[8] pressure,^[9] and oxygen stoichiometry,^[10] can effectively modify the Verwey transition. Among all other attempts, the electric field effect using a conventional field-effect transistor has been tried to modulate the Verwey transition in magnetite epitaxial

1. Introduction

Magnetite (Fe_3O_4) is a model system for understanding strongly correlated oxides.^[1–3] The correlation effect is represented by a metal-to-insulator transition at $T_v = 125$ K, which is well-known as the Verwey transition.^[3] Magnetite crystallizes in the cubic inverse spinel structure (Figure 1a, inset),^[1] where the tetrahedral A sites contain one-third of the Fe ions as Fe^{3+} and the octahedral B sites contain the remaining equal-numbered Fe^{2+} and Fe^{3+} ions. The abrupt Verwey transition, manifested in electrical

Y. Hou, Y. Liu, X. Yang, H. Mao, Q.-L. Ye
Hangzhou Key Laboratory of Quantum Matter
Department of Physics
Hangzhou Normal University
Hangzhou 311121, China
E-mail: qlye@hznu.edu.cn

 The ORCID identification number(s) for the author(s) of this article can be found under <https://doi.org/10.1002/adfm.202104816>.

© 2021 The Authors. Advanced Functional Materials published by Wiley-VCH GmbH. This is an open access article under the terms of the Creative Commons Attribution-NonCommercial-NoDerivs License, which permits use and distribution in any medium, provided the original work is properly cited, the use is non-commercial and no modifications or adaptations are made.

The copyright line for this article was changed on 6 September 2021 after original online publication.

DOI: 10.1002/adfm.202104816

Z. Shi
Shanghai Key Laboratory of Special Artificial Microstructure Materials and Technology & Pohl Institute of Solid State Physics
School of Physics Science and Engineering
Tongji University
Shanghai 200092, China

S. Wu
State Key Laboratory of Optoelectronic Materials and Technologies
School of Materials Science and Engineering
Sun Yat-Sen University
Guangzhou 510275, China

B. Lu
State Key Laboratory of Silicon Materials
Department of Materials Science and Engineering
Zhejiang University
Hangzhou 310027, China

Q.-L. Ye, J. Ye
Device Physics of Complex Materials
Zernike Institute for Advanced Materials
University of Groningen
Nijenborgh 4, Groningen 9747AG, The Netherlands
E-mail: j.ye@rug.nl

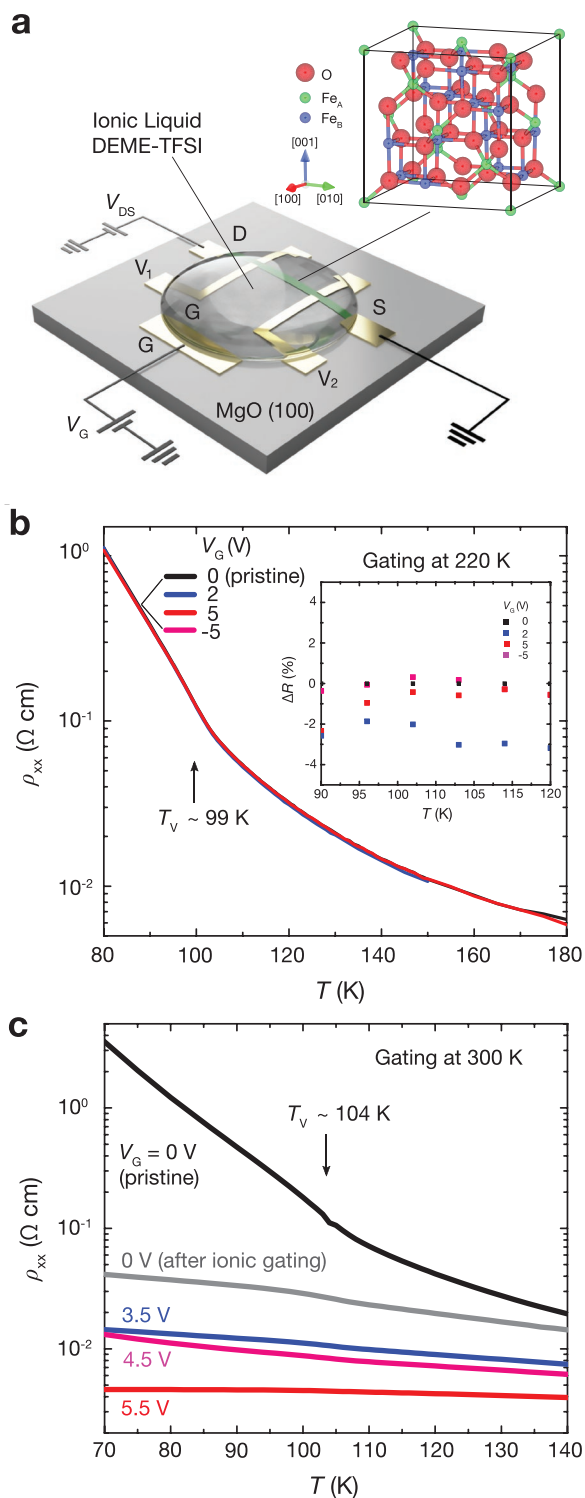


Figure 1. a) Schematic of ionic gating a magnetite device and transport measurement configuration. (Inset) Cubic inverse spinel structure of Fe₃O₄ unit cell. b) Temperature dependence of longitudinal resistivity ρ_{xx} after gating at 220 K, showing negligible changes in the transport features, regardless of the magnitude and polarity of the gate bias. (Inset) Ratios of longitudinal resistance change: $\Delta R = [R(V_G) - R(0)]/R(0) \times 100\%$ for ion-gated states at 220 K. c) Temperature dependence of ρ_{xx} after gating at 300 K, showing significant suppression of ρ_{xx} at low temperature and the disappearing Verwey phase with the increase of positive gate bias.

thin films and single-crystalline nanowires.^[11,12] Nevertheless, limited by the capability of tuning carriers, the conventional field-effect is insufficient to alter the Verwey transition.

To induce a significant modulation, ionic gating stands out as the choice, which can easily reach a field strength $>10 \text{ MV cm}^{-1}$. The carrier doping in the order of $\approx 10^{14} \text{ cm}^{-2}$ can induce quantum phase transitions in insulators,^[13,14] semiconductors,^[15,16] and even noble metals such as Pt.^[17] In addition to the electrostatic operation, ionic gating can also realize carrier doping electrochemically through the creation of oxygen vacancies or the intercalation of protons.^[18–20] Therefore, ionic gating is capable of switching the magnetic and electronic properties of magnetite, although it is yet to be applied.

Here, we report tuning the magnetic and electronic properties of magnetite by ionic gating. By suppressing the Verwey phase, the magnetite exhibits an insulator–metal transition. The induced metallic phase shows a variable sign reversal in the anomalous Hall (AH) coefficient. Our analysis suggests that the insulator-metal transition reflects the metallization of the trimeron state due to the ionic gating, which causes both oxygen vacancies and proton doping. Compared with the carriers in the pristine state, the structural distortion driven by the oxygen vacancies induces a new type of carrier with different spin orientation, causing the sign reversal in the AH coefficient.

2. Results

2.1. Ion-Gated Magnetite Device and its Low-Temperature Transport Properties

The ion-gated magnetite transistors (Figure 1a) are based on the epitaxial magnetite thin films grown on the (100) surface of MgO substrates (by magnetron reactive DC-sputtering in an argon-oxygen mixture). We tune the substrate temperature (200 °C) and oxygen partial pressure (0.01 Pa) to achieve epitaxial growth and stoichiometry (as detailed in Experimental Section and Supporting Information).

The transistor has a Hall bar (300 μm in channel width) and a coplanar side gate, which are shaped by shadow masks (as detailed in Experimental Section and Figure S3, Supporting Information). A widely used ionic liquid (IL): *N,N*-diethyl-*N*-(2-methoxyethyl)-*N*-methylammonium bis-(trifluoromethylsulphonyl)-imide (DEME-TFSI) was chosen as the gating media for its chemical stability, that is, wide electrochemical window.^[13–16,20] The electrical transport was measured in a home-built system tested by the control experiment of gating similar devices with gold channels (as detailed in Experimental Section and Figure S4, Supporting Information).^[21,22] Consistent results were obtained from six ion-gated Fe₃O₄ devices (Device A-F, with their parameters compared in Table S1, Supporting Information).

Figure 1b,c shows the low-temperature transport properties of magnetite at different gated states. Before applying the gate bias (i.e., in the pristine state), all devices (Device A-F) show similar temperature dependences in the longitudinal resistivities ρ_{xx} : the ρ_{xx} increases with the decrease of temperature and displays a steep rise at the $T_v = 99\text{--}114 \text{ K}$, which is determined by the minimum found in the plot of $d\log(\rho_{xx})/dT$ versus T . The T_v found in thin films (even with exact stoichiometric films)

grown on MgO(100) are consistently lower and broader than the bulk T_V . This is caused by the inevitable occurrence of antiphase boundaries (APBs) as reported in previous studies (Figure S2c, Supporting Information).^[10,23,24] After applying the gate voltage V_G at 220 K (for Device B), and holding the V_G while cooling down, the Verwey feature found in ρ_{xx} is not noticeably affected regardless of the magnitude and polarity of the V_G (Figure 1b). The ratio of resistance change $\Delta R = [R(V_G) - R(0)]/R(0) \times 100\%$ is less than 4% (the inset of Figure 1b). The drain-source current I_{DS} is also nearly V_G independent (Figure S5a, Supporting Information). All these results indicate that the electrostatic gating at 220 K cannot affect the Verwey transition, which agrees with the previous report.^[11]

On the other hand, when the identical protocol is repeated by applying the V_G at 300 K, the ρ_{xx} (Device C) at low temperature decreased significantly with the increase of V_G showing a phase transition from insulator to metal. The Verwey phase with a high resistivity is almost suppressed for $V_G > 4.5$ V (Figure 1c). After removing the gate voltage (i.e., setting $V_G = 0$ V) and warm up the device back to 300 K, the following measurement of the temperature dependence of ρ_{xx} at $V_G = 0$ V can only partially restore the pristine resistivity. This irreversible change is further verified by the transfer curve (Figure S5a, Supporting Information).

To understand the underlying mechanism for the irreversible change in the ion-gated magnetite at 300 K, we further measured the temporal response of drain-source current I_{DS} to the

V_G . For gating at 300 K (Figure 2a), the I_{DS} shows an accumulative dependence on the ON/OFF cycles of $V_G = 4.0$ V. The I_{DS} increases sharply when V_G is ON, while decreases gradually and saturates at a larger I_{DS} , which is not reversible compared to the I_{DS} measured when V_G is OFF. Due to the partial recovery, the I_{DS} progressively increases after experiencing more ON/OFF cycles. The cyclic gating response closely follows the gating history, which is fundamentally different from the repeatable behaviors observed in electrostatic charge accumulation.^[13–17,21,22] This suggests that the mechanism of resistivity reduction by gating at 300 K involves electrochemical effects such as gate-induced oxygen vacancy and proton (H^+) doping.^[18–20] In Figure 2b, we further explored the temporal response of the I_{DS} at a fixed gate voltage. For both $V_G = 5.0$ and 5.5 V (applied at 300 K), the I_{DS} increases sharply within the first a few minutes, which is then followed by a gradual increase for a longer period before showing an even larger increase after more than 1 h of gating. These gating stages clearly show two different electrochemical processes with distinct temporal responses. Therefore, compared with V_G , the I_{DS} then becomes the more direct guidance to characterize different gating stages. As shown in Figure 2c, the temperature dependence of ρ_{xx} (Device D), guided by the increase of I_{DS} at 300 K, shows a remarkable reduction at low temperature. This result is consistent with the data shown in Figure 1c, indicating that the higher I_{DS} measured at room temperature corresponds to a stronger gate-induced electrochemical reaction.

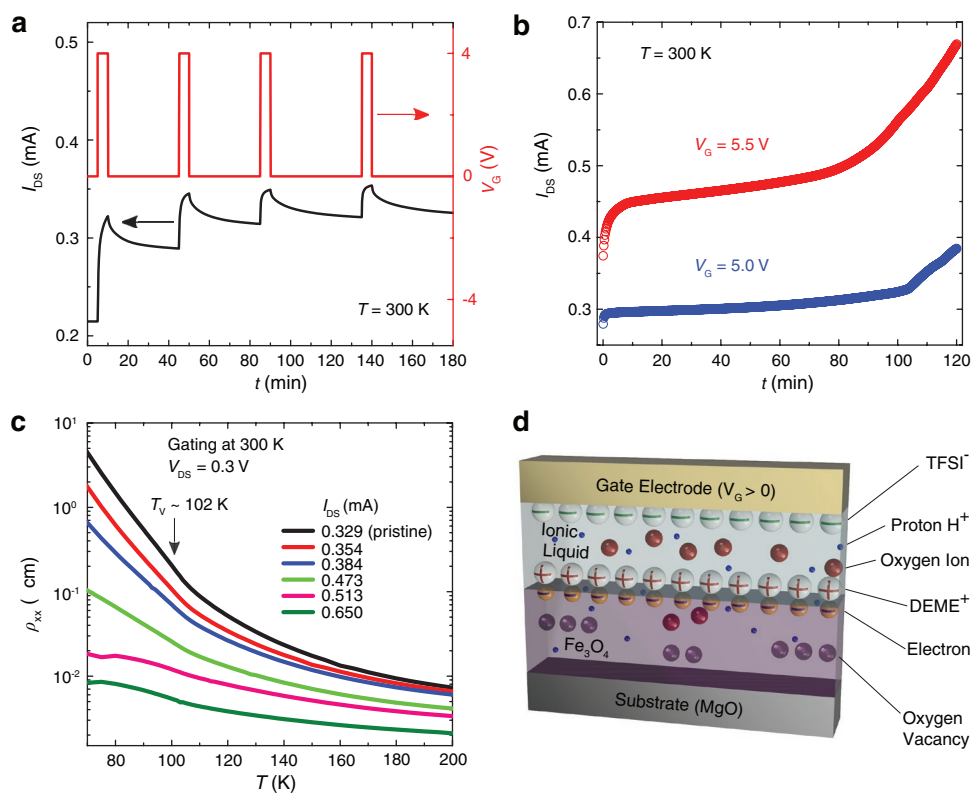


Figure 2. a) Temporal response of drain-source current I_{DS} to the “ON/OFF” cycles of $V_G = 4$ V at 300 K. b) Temporal changes in the I_{DS} at $V_G = 5.0$ and 5.5 V applied at 300 K. c) Temperature dependence of ρ_{xx} at different gating states. The states are characterized by their different I_{DS} values measured as function time at 300 K and a constant gate voltage. Progressively, the state with higher I_{DS} shows a larger decrease of the resistivity at low temperature and stronger suppression of the Verwey phase. d) Schematic illustration of the possible electrochemical effects including migration of proton (H^+) and creation of oxygen vacancies in the magnetite channel during the ionic gating at 300 K.

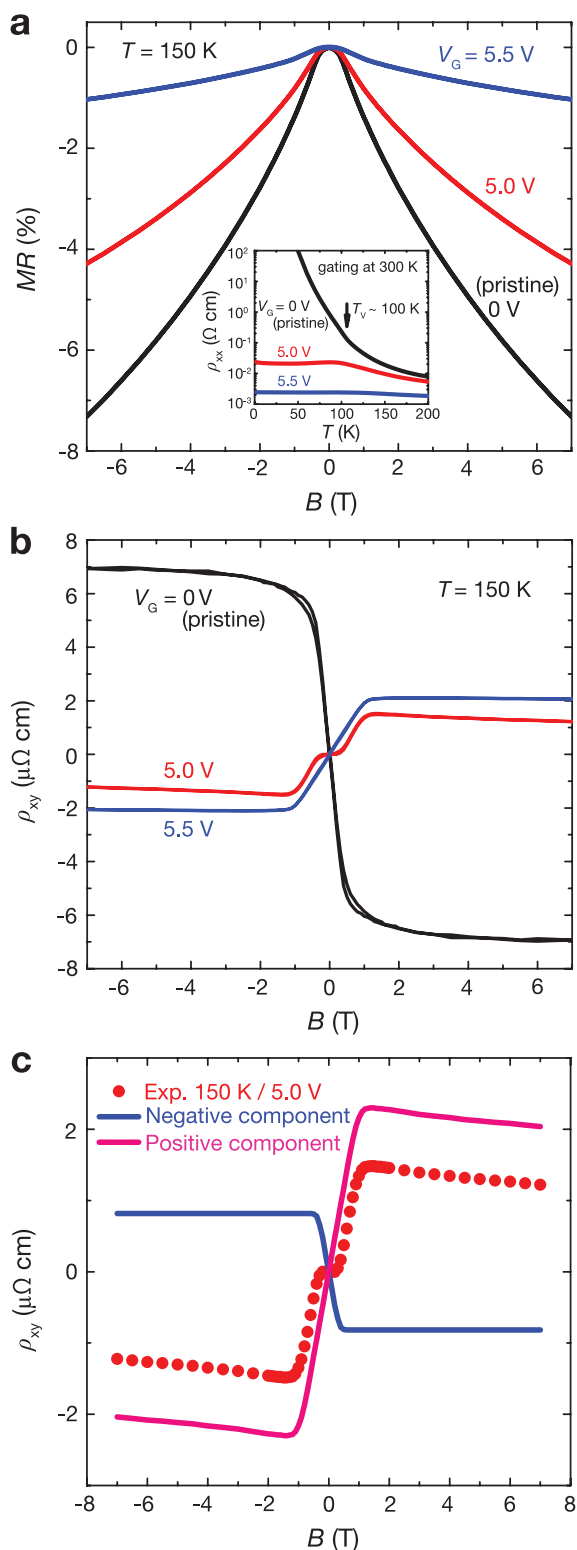


Figure 3. a) MR ratio showing a decrease of MR ratio with the increase of gate bias. (Inset) Temperature dependence of ρ_{xx} after gating at 300 K, showing a significant decrease of the resistivity at low temperature with the increase of positive gate bias. b) Magnetic field dependence of Hall resistivity ρ_{xy} , showing a sign reversal of the AH coefficient after ionic gating. c) Magnetic field dependence of Hall resistivity ρ_{xy} gated at $V_G =$

The aforementioned results suggest the following mechanism shown schematically in Figure 2d for the ionic gating at 300 K. After applying a positive gate bias, the protons (H^+) dissolved in IL can be intercalated into the magnetite channel due to their small size.^[20] Meanwhile, the strong electric field in the Helmholtz double layer is also sufficient to drive oxygen slowly out of the oxide (Fe_3O_4) into the IL, consequently, creating oxygen vacancies in the magnetite channel.^[18,19] The gate-induced proton intercalation and oxygen-vacancy generation both have an electrochemical nature, which is the main cause of the decrease of ρ_{xx} at low temperatures shown in Figures 1c and 2c.^[19,20] When V_G is reduced to 0 V, a reversible proton exchange is expected because the small protons can easily diffuse away from the magnetite channel and return to the IL, which is analogous to the discharge process of a secondary battery.^[20] Whereas, once created, the oxygen vacancies are more stable in the channel.^[18] Hence, ρ_{xx} can recover only partially (Figures 1c and 2). Although both electrochemical processes are assisted by the electrostatic effect due to the formation of a Helmholtz double layer, field-driven proton doping appears to be the dominating process in our device in a time scale shorter than 1 h. The reversible proton exchange between the IL and channel is accompanied by the creation of oxygen vacancies, taking an even longer time, and is responsible for the irreversible part in the electrical properties.

2.2. Magnetotransport and Sign Reversal of the AH Coefficient

The presence of gate-induced oxygen vacancies can disturb stoichiometry. Recent reports show that oxygen vacancies in Fe_3O_4 thin films can increase spin-orbit coupling,^[25] introducing a gapped state and spin-flipping.^[26,27] As a result, it is highly expected that the electrochemical processes discussed above can also change spin-related properties in magnetite and significantly influence magnetotransport. Since the state of the gated device can only be partially recovered due to the electrochemical effects, to study the magnetotransport, we prepared an identical device (Device E) that shows a similar temperature dependence with $T_v \approx 100$ K and started from the pristine state (the inset of Figure 3a, similar as results observed in all devices). Take the I_{DS} as guidance, we reach the states shown in Figures 1c and 2c for the magnetoresistance (MR) and Hall resistivity by applying a magnetic field B perpendicular to the channel surface. As shown in Figure 3a, the MR ratios, defined as

$$MR = \frac{[\rho_{xx}(B) - \rho_{xx}(0)]}{\rho_{xx}(0)} \times 100\% \quad (1)$$

were measured above the Verwey transition at 150 K for different gating states. In the pristine state, the MR shows a non-saturated negative value of $\approx 7\%$ at the maximum field of ± 7 T. The MR exhibits a quadratic field dependence at low field, due to the existence of the sharp antiferromagnetic APBs in the magnetite thin film grown on MgO substrate (see

5.0 V (red dots, the same as the red curve in b). A plateau is observed within the low fields of ± 0.2 T, which can be separated into a negative AH component (blue curve) and a positive AH component (pink curve), using the analysis reported in Ref. [29].

Figure S2c, Supporting Information).^[28] After the ionic gating, while keeping the quadratic low-field dependences, the MR decreases with the gating voltage, and the maximum value of MR (± 7 T) in the state prepared by $V_G = 5.5$ V is reduced to $\approx 1\%$. Identical behavior was observed in the MR curves measured at 100 K for the different gating states of the device (Figure S6a, Supporting Information). As shown in the inset of Figure 3a, the ρ_{xx} increases significantly for the pristine state below the Verwey transition, affecting the accuracy of the Hall effect and MR. Therefore, we choose to compare magnetotransport at high temperatures.

As shown in Figure 3b, the Hall resistivity ρ_{xy} measured at 150 K can be described by an empirical relationship:

$$\rho_{xy} = R_O B + R_A \mu_0 M \quad (2)$$

where R_O and R_A are the ordinary and AH coefficients, respectively. The M is the spontaneous magnetization, and μ_0 is the vacuum permeability. In the pristine state, the ordinary Hall coefficient R_O is negative for the electron transport, and the AH coefficient R_A is also negative, which is consistent with the previous report of the epitaxial magnetite thin films.^[23,24] After the ionic gating at 300 K, the sign of the AH coefficient R_A is surprisingly reversed from negative to positive, while the ordinary Hall coefficient R_O remains negative, indicating the type of the conduction carrier remains to be electron. A closer look at the Hall resistivity ρ_{xy} shows that there exists a plateau in the low field of ± 0.2 T for the gating state accessed at $V_G = 5.0$ V. As shown in Figure 3c, the plateau indicates an intermediate state in the process of sign reversal, which can be separated into two components:^[29] a negative R_A coming from the pristine state and a positive R_A developed after ionic gating. As being further gated at 5.5 V, the AH resistivity completely reversed to positive without further showing any plateaus. It is worth noting that although the sign reversal of R_A can be resolved at 150 K above the T_v , the characteristic plateau disappears at 100 K (Figure S6b, Supporting Information) for the same state accessed at $V_G = 5.0$ V. This indicates that the positive R_A induced by ionic gating supersedes the contribution of negative R_A from the pristine state and dominates the low-temperature behavior. Namely, for the state with positive R_A at 100 K, its sign reversal is completed either in a lower gating state or at a higher temperature.^[30] On the other hand, this also supports our choice to compare the magnetotransport at 150 K, at which the competing behavior can display fully.

The AH effect (AHE) arising from spin-orbit interactions has been addressed in theories considering the intrinsic and extrinsic mechanisms.^[31–33] A fruitful method experimentally testing the different mechanisms is by measuring the scaling between the AH conductivity σ_{xy}^{AH} and the longitudinal conductivity σ_{xx} . For the cubic symmetry in magnetite and perpendicularly applied magnetic field, we can obtain

$$|\sigma_{xy}^{AH}| = |\rho_{xy}^{AH}| / [(\rho_{xx})^2 + (\rho_{xy}^{AH})^2] \quad (3)$$

and

$$\sigma_{xx} = \rho_{xx} / [(\rho_{xx})^2 + (\rho_{xy}^{AH})^2]. \quad (4)$$

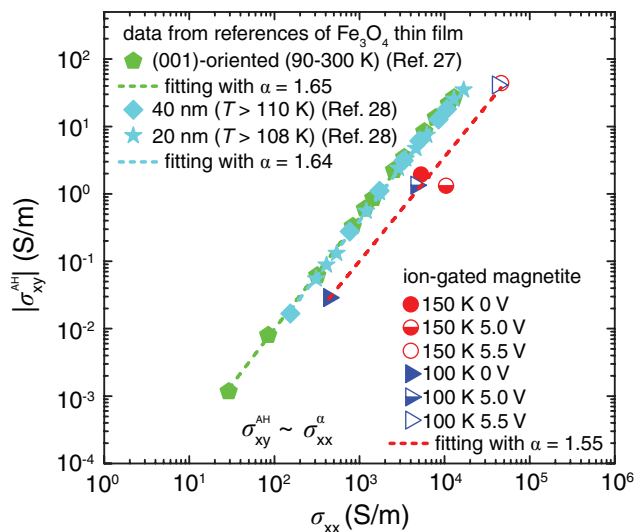


Figure 4. Relationship between the magnitude of the AH conductivity $|\sigma_{xy}^{AH}| = |\rho_{xy}^{AH}| / [(\rho_{xx})^2 + (\rho_{xy}^{AH})^2]$ and the longitudinal conductivity $\sigma_{xx} = \rho_{xx} / [(\rho_{xx})^2 + (\rho_{xy}^{AH})^2]$ for ion-gated magnetite at different gating states, which are compared with the data measured in similar systems: from Ref. [23] for the (001)-oriented epitaxial Fe_3O_4 thin film grown on MgO (001) by laser molecular-beam epitaxy and from Ref. [24] for the epitaxial Fe_3O_4 thin films (thickness of 40 and 20 nm) grown on MgO (001) by pulsed laser deposition. The scaling relationship in the power-law form of $\sigma_{xy}^{AH} \propto \sigma_{xx}^\alpha$. The best fitting shows the exponent $\alpha = 1.55$, which is consistent with the theoretical value of 1.6. The identical scaling exponent α is found in all accessed states after ionic gating at 300 K.

In the present system, we cannot obtain the ρ_{xy}^{AH} by extrapolating the linear part of ρ_{xy} (B) at high field back to the zero field. This is because the magnetization does not saturate at the high field due to the presence of the APBs. The Hall resistivity at the maximum magnetic field of 7 T can be a good approximation of the ρ_{xy}^{AH} , that is, $\rho_{xy}^{AH} \approx \rho_{xy}(7 \text{ T})$, since the ordinary Hall resistivity ρ_{xy}^{OH} becomes negligibly small compared with the ρ_{xy}^{AH} value.^[23,24] Figure 4 shows the relationship between the σ_{xy}^{AH} and σ_{xx} for magnetite at different gating states and temperatures (Figure 3b and Figure S6b, Supporting Information), which is compared with reference materials take from Refs. [23] and [24]. By fitting our data with the scaling relationship in the power-law form: $\sigma_{xy}^{AH} \propto \sigma_{xx}^\alpha$, the best-fitting yields exponent $\alpha = 1.55$, regardless of different gating states. The value of our fitting exponent α is close to the theoretically predicted value of 1.6.^[33] This indicates that the AHE in our device is caused by the damping of the intrinsic contribution in the dirty regime.^[23,24,33] The consistent power-law dependence obtained in the scaling for different levels of oxygen vacancy and/or doping of protons further confirms the universality in the scaling relationship in our devices.^[23,24]

3. Discussion

As shown in Figures 2 and 3, the low-temperature transport of ion-gated magnetite film shows two main results: 1) a clear suppression of the Verwey phase due to the formation of

conduction channels with higher conductivity after ionic gating and 2) a gating-dependent sign reversal of AHE in the process of establishing this new conduction channel. The nearly metallic low-temperature state shown in Figure 2 is induced by suppressing the Verwey phase. As shown in the further analysis (Figure S7, Supporting Information), the gating-enhanced conductivity is established on the pristine insulating trimeron states. Instead of a gradual weakening the Verwey transition, the suppression of the insulating state is manifested as a process of building up an enhancing conduction channel that sets in at ≈ 80 K. In all gated states, although the Verwey transition becomes weaker and broader, there always exists a contribution from the pristine Verwey transition close to T_V . These transport signatures indicate that, by destroying the uniform trimeron state, an increasingly metallic network is gradually formed by gating, which bypasses the insulating Verwey regions that remain unchanged after gating. Consistently, the contribution from the pristine Verwey phase, that is, the dip corresponding to T_V (Figure S7, Supporting Information) in the temperature dependence of $d\log(\rho_{xx})/dT$, diminishes in the gate-induced states with enhanced conductivity.

The sign reversal of the AH coefficient has been experimentally observed in many magnetic systems as a function of chemical doping,^[29,34–36] and electric-field gating.^[37,38] Various mechanisms have been proposed theoretically.^[39,40] The phenomenological theory relates the sign change to a change of the effective spin-orbit coupling with varying chemical potential.^[39] On the other hand, it was shown that doping-induced sign reversal observed in $\text{CuCr}_2\text{Se}_{4-x}\text{Br}_x$ is due to the change of Berry-phase,^[36] that is, the appearance of the sharp and spiky features in the sum of Berry curvature of the occupied bands, which varies with the dopant concentration.^[40]

In ion-gated magnetite, the ordinary Hall coefficient remains electron-like. Therefore, we can exclude a global change in Fermi surface topology as the origin of sign reversal. Also, the contribution from skew scattering to the AHE is negligible in our device, because the contribution from skew scattering is dominant in the clean regime. Furthermore, according to the magnetic properties and XPS spectra of the ion-gated devices, the formation of FeO and/or Fe phases can be safely excluded (Figures S9 and S10, Supporting Information). As shown in the universal scaling relation (Figure 4), by excluding the mechanisms discussed above, the AHE of our device is most likely originated from the intrinsic mechanism related to the Berry-phase curvature of magnetite, which contributes regardless of the gating state. In the pristine state, only the minority down-spin electrons of Fe^{2+} on *B* sites act as the conduction carriers, and the AH coefficient is negative. After ionic gating at 300 K, the creation of oxygen vacancy by the electrochemical gating may cause the partial reduction of Fe^{3+} to Fe^{2+} (Figure S10, Supporting Information), and induce a structural distortion as reported in similar correlated oxides.^[18–20,41] Hence, the doped electrons are a new type of carrier having a minority spin-up state that appears on the *A* sites. Consistently, a similar contribution to the transport was previously reported in the high-temperature magnetotransport of magnetite single crystals.^[42] Since the AHE is closely related to the spin-dependent scattering of carriers through spin-orbit interaction, the sign reversal of the AHE in our

ion-gated devices can be attributed to the newly induced carriers at the *A* sites with a competing spin that orientated oppositely to that in the pristine state.

4. Conclusion

In conclusion, we have utilized ionic gating to tune the low-temperature insulating Verwey state into metallic continuously, which also causes the reversal of the sign of the AH coefficient. The tuning of magnetic and electronic properties of magnetite is driven by the ion-gating induced proton additions and oxygen vacancies which result in the variable structural distortions and hence the modulation of orbital configurations. Recent work has shown that the trimeron correlations can persist well above T_V up to 300 K and even higher temperatures.^[43] Hence the changes in transport properties by ionic gating at 300 K may already reflect the breaking up of the trimeron states. Namely, the proton additions and oxygen vacancies at room temperature can already form a glassy disordered state that leads to metallization. The ionic gating provides a simple and effective method to tune the low-temperature correlated state, which is crucial for the further study of the Verwey and similar correlation transitions.

5. Experimental Section

Preparation of Epitaxial Fe_3O_4 Thin Films: The epitaxial thin films of magnetite (Fe_3O_4) were grown by magnetron reactive DC-sputtering in the presence of an argon-oxygen gas mixture (100:2). High purity (99.99%) Fe and one-side polished MgO (100) single crystals were used as the sputtering source and growth substrates, respectively. The MgO (100) substrates were first heated to 600 °C with a rate of 10 °C min^{-1} and kept for 2.5 h at 600 °C to eliminate any possible contamination on the surface and hence ensure a good film-substrate interface. The key parameters of substrate temperature and oxygen partial pressure for the epitaxial growth of stoichiometric Fe_3O_4 thin films were optimized as discussed in Figures S1 and S2, Supporting Information.

Devices Fabrication: The main procedures to make magnetite devices for ionic gating are illustrated in Figure S3, Supporting Information. First, a Hall bar-shaped Fe_3O_4 film was deposited on MgO (100) substrate ($5 \times 5 \times 0.5$ mm³), using a shadow mask with a length of 3 mm and a width of 300 μm (Figure S3a, Supporting Information). Afterward, Ti (10 nm)/Au (50 nm) electrodes were deposited by magnetron DC-sputtering, for both current/voltage probes and co-planar side gate by aligning a shadow mask for electrodes with the Hall bar channels (Figure S3b, Supporting Information). The effective channel length between the centers of the two electrodes for measuring longitudinal voltage V_{xx} is 400 μm . The prepared devices were then attached to the PPMS sample puck by silver paste (Figure S3c, Supporting Information). Finally, a small droplet of ionic liquid (DEME-TFSI, Kanto Chemical Co.), serving as the ionic media, was applied to cover both the film channel and the gate electrode to complete the device (Figure S3d, Supporting Information).

Electrical Transport Measurements: The electrical transport was measured in a Physical Property Measurement System (PPMS-9, Quantum Design). The resistance of the pristine Fe_3O_4 film was in the $\text{M}\Omega$ range after the Verwey transition. Therefore, a small $V_{DS} = 0.3$ V was applied to minimize the Joule heating.^[44] The sweep rate of the gate bias is 10 mV s^{-1} . All electrodes show ohmic contact to the film verified by their linear I/V response. The temperature dependence of resistivities was measured in the warming-up process for a fixed ionic gating state set at 220 or 300 K. To measure magnetic field dependences of MR and Hall resistivity shown in Figure 3 and Figure S6, Supporting Information,

the device was firstly applied with a smaller fixed gate voltage (e.g., 5.0 V) at 300 K for 2 h. A constant current of 100 μ A was used for all the magnetotransport measurements. The measurement parameters for all devices are summarized in Table S1, Supporting Information.

Structural Characterizations: X-ray diffraction (XRD) was measured for the out-of-plane θ - 2θ scans. And the rocking curves were measured on a Bruker D8 XRD with Ψ/Φ scan. Raman spectra were measured by Micro-Raman Spectrometer (Renishaw inVia). And the X-ray photoelectron spectroscopy (Kratos AXIS Supra) was measured using the K_{α} (1253.6 eV) line of Mg. The magnetization of the thin film was measured by Magnetic Property Measurement System (MPMS-VSM, Quantum Design) for characterizing the sample quality.

Supporting Information

Supporting Information is available from the Wiley Online Library or from the author.

Acknowledgements

We thank the technical support from Joost Zoestbergen. This work was supported by the National Natural Science Foundation of China (Grant No. 11774259, 12074285), the National Science Foundation of Zhejiang Province (Grant No. LY17A040009, LY18F010019), the Key Research and Development Program of Zhejiang Province (Grant No. 2021C01030), the Natural Science Foundation of Guangdong Province (Grant No. 2021A1515012381), the Science and Technology Planning Project of Guangzhou City (Grant No. 202102080605), the China Scholarship Council (Grant No. 201908330139), and the European Research Council (Consolidator Grant No. 648855, Ig-QPD).

Conflict of Interest

The authors declare no conflict of interest.

Keywords

anomalous Hall effect, ionic gating, strongly correlated oxide, Verwey transition

Received: May 20, 2021

Revised: August 2, 2021

Published online: August 26, 2021

[1] E. J. W. Verwey, J. H. de Boer, *Rec. Trav. Chim.* **1936**, 55, 531.

[2] M. A. Gillo, *Phys. Rev.* **1958**, 109, 777.

[3] E. J. W. Verwey, *Nature* **1939**, 144, 327.

[4] M. S. Senn, J. P. Wright, J. P. Attfield, *Nature* **2012**, 481, 173.

[5] S. de Jong, R. Kukreja, C. Trabant, N. Pontius, C. F. Chang, T. Kachel, M. Beye, F. Sorgenfrei, C. H. Back, B. Bräuer, W. F. Schlotter, J. J. Turner, O. Krupin, M. Doehler, D. Zhu, M. A. Hossain, A. O. Scherz, D. Fausti, F. Novelli, M. Esposito, W. S. Lee, Y. D. Chuang, D. H. Lu, R. G. Moore, M. Yi, M. Trigo, P. Kirchmann, L. Pathey, M. S. Golden, M. Buchholz, P. Metcalf, F. Parmigiani, W. Wurth, A. Föhlich, C. Schüßler-Langeheine, H. A. Dürr, *Nat. Mater.* **2013**, 12, 882.

[6] R. Kukreja, N. Hua, J. Ruby, A. Barbour, W. Hu, C. Mazzoli, S. Wilkins, E. E. Fullerton, O. G. Shpyrko, *Phys. Rev. Lett.* **2018**, 121, 177601.

[7] V. A. M. Brabers, F. Walz, H. Kronmüller, *Phys. Rev. B* **1998**, 58, 14163.

[8] M. Liu, J. Hoffman, J. Wang, J. Zhang, B. Nelson-Cheeseman, A. Bhattacharya, *Sci. Rep.* **2013**, 3, 1876.

[9] S. Todo, N. Takeshita, T. Kanehara, T. Mori, N. Mori, *J. Appl. Phys.* **2001**, 89, 7347.

[10] X. H. Liu, A. D. Rata, C. F. Chang, A. C. Komarek, L. H. Tjeng, *Phys. Rev. B* **2014**, 90, 125142.

[11] J. J. I. Wong, A. G. Swartz, R. Zheng, W. Han, R. K. Kawakami, *Phys. Rev. B* **2012**, 86, 060409(R).

[12] J. Gooth, R. Zierold, J. G. Glusckhe, T. Boehnert, S. Edinger, S. Barth, K. Nielsch, *Appl. Phys. Lett.* **2013**, 102, 073112.

[13] J. T. Ye, S. Inoue, K. Kobayashi, Y. Kasahara, H. T. Yuan, H. Shimotani, Y. Iwasa, *Nat. Mater.* **2010**, 9, 125.

[14] J. T. Ye, Y. J. Zhang, R. Akashi, M. S. Bahramy, R. Arita, Y. Iwasa, *Science* **2012**, 338, 1193.

[15] J. M. Lu, O. Zheliuk, I. Leermakers, N. F. Q. Yuan, U. Zeitler, K. T. Law, J. T. Ye, *Science* **2015**, 350, 1353.

[16] Y. J. Zhang, T. Oka, R. Suzuki, J. T. Ye, Y. Iwasa, *Science* **2014**, 344, 725.

[17] L. Liang, Q. Chen, J. Lu, W. Talsma, J. Shan, G. R. Blake, T. T. M. Palstra, J. T. Ye, *Sci. Adv.* **2018**, 4, eaar2030.

[18] J. Jeong, N. Aetukuri, T. Graf, T. D. Schladt, M. G. Samant, S. S. P. Parkin, *Science* **2013**, 339, 1402.

[19] S. Chen, X. Wang, L. Fan, G. Liao, Y. Chen, W. Chu, L. Song, J. Jiang, C. Zou, *Adv. Funct. Mater.* **2016**, 26, 3532.

[20] K. Shibuya, A. Sawa, *Adv. Electron. Mater.* **2016**, 2, 1500131.

[21] D. Daghero, F. Paolucci, A. Sola, M. Tortello, G. A. Ummarino, M. Agosto, R. S. Gonnelli, J. R. Nair, C. Gerbaldi, *Phys. Rev. Lett.* **2012**, 108, 066807.

[22] H. Nakayama, J. T. Ye, T. Ohtani, Y. Fujikawa, K. Ando, Y. Iwasa, E. Saitoh, *Appl. Phys. Express* **2012**, 5, 023002.

[23] D. Venkateshvaran, W. Kaiser, A. Boger, M. Althammer, M. S. Ramachandra Rao, S. T. B. Goennenwein, M. Opel, R. Gross, *Phys. Rev. B* **2008**, 78, 092405.

[24] A. Fernández-Pacheco, J. M. De Teresa, J. Orna, L. Morellon, P. A. Algarabel, J. A. Pardo, M. R. Ibarra, *Phys. Rev. B* **2008**, 77, 100403(R).

[25] Z. Huang, W. Liu, J. Yue, Q. Zhou, W. Zhang, Y. Lu, Y. Sui, Y. Zhai, Q. Chen, S. Dong, J. Wang, Y. Xu, B. Wang, *ACS Appl. Mater. Interfaces* **2016**, 8, 27353.

[26] R. Arras, L. Calmels, B. Warot-Fonrose, *Appl. Phys. Lett.* **2012**, 100, 032403.

[27] A. D. Fauzi, M. A. Majidi, A. Rusydi, *J. Phys.: Condens. Matter* **2017**, 29, 135802.

[28] W. Eerenstein, T. T. M. Palstra, S. S. Saxena, T. Hibma, *Phys. Rev. Lett.* **2002**, 88, 247204.

[29] N. Liu, J. Teng, Y. Li, *Nat. Commun.* **2018**, 9, 1282.

[30] S. Shimizu, K. S. Takahashi, T. Hatano, M. Kawasaki, Y. Tokura, Y. Iwasa, *Phys. Rev. Lett.* **2013**, 111, 216803.

[31] N. Nagaosa, J. Sinova, S. Onoda, A. H. MacDonald, N. P. Ong, *Rev. Mod. Phys.* **2010**, 82, 1539.

[32] D. Xiao, M. C. Chang, Q. Niu, *Rev. Mod. Phys.* **2010**, 82, 1959.

[33] S. Onoda, N. Sugimoto, N. Nagaosa, *Phys. Rev. Lett.* **2006**, 97, 126602.

[34] D. Li, G. Wang, H. Li, S. Wu, S. Li, *Mater. Res. Bull.* **2020**, 122, 110646.

[35] T. Golod, A. Rydh, P. Svedlindh, V. M. Krasnov, *Phys. Rev. B* **2013**, 87, 104407.

[36] W. L. Lee, S. Watauchi, V. L. Miller, R. J. Cava, N. P. Ong, *Science* **2004**, 303, 1647.

[37] L. Liang, J. Shan, Q. H. Chen, J. M. Lu, G. R. Blake, T. T. M. Palstra, G. E. W. Bauer, B. J. van Wees, J. T. Ye, *Phys. Rev. B* **2018**, 98, 134402.

[38] S. Zhang, R. Wang, X. Wang, B. Wei, B. Chen, H. Wang, G. Shi, F. Wang, B. Jia, Y. Ouyang, F. Xie, F. Fei, M. Zhang, X. Wang,

- D. Wu, X. Wan, F. Song, H. Zhang, B. Wang, *Nano Lett.* **2020**, *20*, 709.
- [39] P. Nozières, C. Lewiner, *J. Phys.* **1973**, *34*, 901.
- [40] Y. Yao, Y. Liang, D. Xiao, Q. Niu, S.-Q. Shen, X. Dai, Z. Fang, *Phys. Rev. B* **2007**, *75*, 020401(R).
- [41] B. Cui, C. Song, G. A. Gehring, F. Li, G. Wang, C. Chen, J. Peng, H. Mao, F. Zeng, F. Pan, *Adv. Funct. Mater.* **2015**, *25*, 864.
- [42] S. Todo, K. Siratori, S. Kimura, *J. Phys. Soc. Jpn.* **1995**, *64*, 2118.
- [43] G. Perversi, E. Pachoud, J. Cumby, J. M. Hudspeth, J. P. Wright, S. A. J. Kimber, J. P. Attfield, *Nat. Commun.* **2019**, *10*, 2857.
- [44] A. A. Fursina, R. G. S. Sofin, I. V. Shvets, D. Natelson, *Phys. Rev. B* **2009**, *79*, 245131.